



OPEN

Computational exploration of copper catalyzed vinylogous aerobic oxidation of unsaturated compounds

Ting Wang¹, Yu Zhou^{1,2}, Yao Xu^{1,2} & Gui-Juan Cheng¹✉

Selective oxidation is one of the most important and challenging transformations in both academic research and chemical industry. Recently, a highly selective and efficient way to synthesize biologically active γ -hydroxy- α,β -unsaturated molecules from Cu-catalyzed vinylogous aerobic oxidation of α,β - and β,γ -unsaturated compounds has been developed. However, the detailed reaction mechanism remains elusive. Herein, we report a density functional theory study on this Cu-catalyzed vinylogous aerobic oxidation of γ,γ -disubstituted α,β - and β,γ -unsaturated isomers. Our computational study unveils detailed mechanism for each elementary step, i.e. deprotonation, O₂ activation, and reduction. Besides, the origin of regioselectivity, divergent reactivities of substrates as well as reducing agents, and the byproduct generation have also been investigated. Notably, the copper catalyst retains the +2 oxidation state through the whole catalytic cycle and plays essential roles in multiple steps. These findings would provide hints on mechanistic studies and future development of transition metal-catalyzed aerobic oxidation reactions.

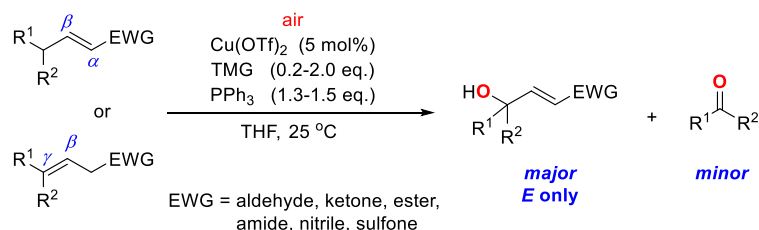
Selective oxidation has gained a preeminent position in both academic research and chemical industry^{1–3}. One particular class of selective oxidation reactions achieved by a combined use of air as an oxidant and copper as a catalyst is highly desirable due to the natural abundance of air and copper^{4–6}. Over the past few decades, great progress has been made in this field and many successful Cu-catalyzed aerobic reactions have been developed^{7–23}.

Catalytic vinylogous reactions are among the most important reactions in organic synthesis due to their extensive application in the synthesis of complex natural products and bioactive molecules^{24–27}. Despite significant advances in transition metal-catalyzed α - or β -functionalization of α,β - and β,γ -unsaturated compounds^{28–32}, the vinylogous version leading to synthetically valuable γ -substituted α,β -unsaturated compounds^{33–36} has been rarely studied. For example, the vinylogous hydroxylation of α,β -unsaturated or β,γ -unsaturated compounds is a direct method to synthesize γ -hydroxy- α,β -unsaturated compounds^{37–42} which are valuable biological active pharmaceuticals and important intermediates in organic synthesis. However, the catalytic aerobic vinylogous hydroxylation is highly challenging due to the control of the reaction selectivity^{43,44}, such as regioselectivity, chemoselectivity (hydroxylation vs. oxidative fragmentation, epoxidation, and other competitive oxidation reactions) and overoxidation problems.

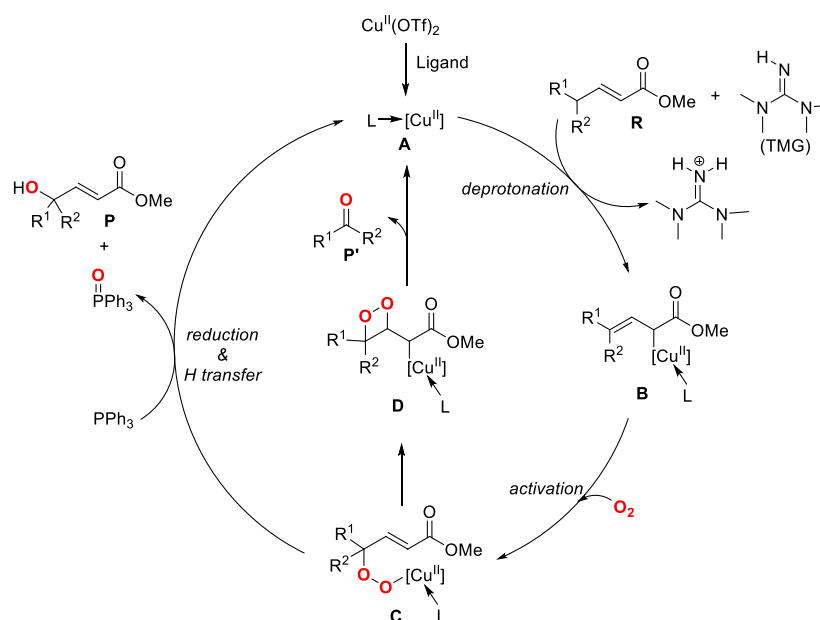
In 2018, Yin and Newhouse's group successfully realized an efficient and operationally simple copper-catalyzed vinylogous oxidation reaction by using air as an oxidant, which leads to a broad array of γ -hydroxy- α,β -(*E*)-unsaturated compounds⁴⁵. Reactions of both γ,γ -disubstituted α,β - and β,γ -unsaturated compounds produce γ -hydroxy- α,β -(*E*)-unsaturated compounds in high yield with perfect stereo- and regioselectivity (Scheme 1). The copper(II) triflate catalyst, the base (tetramethylguanidine, TMG), and the reducing agent (PPh₃) were found essential for the reaction. Their method was successfully applied to the vinylogous oxidation of unsaturated esters, aldehydes, ketones, amides, nitriles, and sulfones, demonstrating great potential in the synthesis of natural products and bioactive molecules.

The preliminary mechanistic study indicated that radicals might not be involved in the reaction because the reaction efficiency was not affected by the addition of radical scavengers^{46–48}. Based on the experimental observations, Yin et al. proposed a three-step pathway for the generation of the main γ -hydroxylated product (Scheme 2).

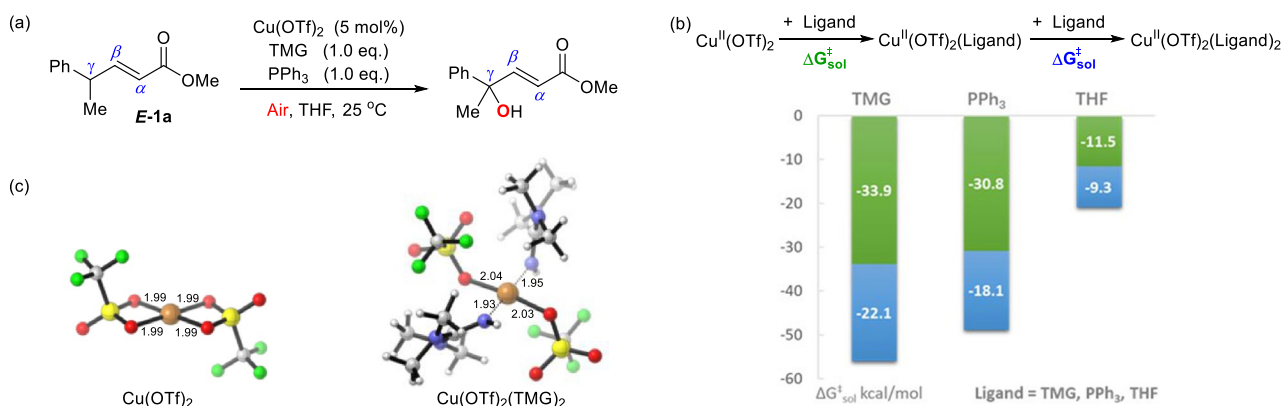
¹Warshel Institute for Computational Biology, Shenzhen Key Laboratory of Steroid Drug Development, School of Life and Health Sciences, The Chinese University of Hong Kong (Shenzhen), Shenzhen 518172, China. ²School of Life Sciences, University of Science and Technology of China, Hefei 230027, Anhui, China. ✉email: chengguijuan@cuhk.edu.cn



Scheme 1. Copper-catalyzed vinylogous aerobic oxidation of γ,γ -disubstituted α,β - and β,γ -unsaturated compounds.



Scheme 2. Proposed reaction mechanism for the copper-catalyzed vinylogous aerobic oxidation.



Scheme 3. (a) The Representative Reaction for the DFT Calculation. (b) Binding of TMG, PPh_3 , and THF with $Cu^{II}(OTf)_2$. Binding Free Energies Are in kcal/mol. (c) The Structures of $Cu^{II}(OTf)_2$ and $Cu^{II}(OTf)_2(TMg)_2$. Bond Distances Are Given in Angstroms (\AA). Note CYLview, 1.0b, <https://www.cylview.org/download.html>.

This pathway consists of deprotonation ($A + R + TMG \rightarrow B$), O_2 activation ($B + O_2 \rightarrow C$) and PPh_3 participated reduction step ($C + PPh_3 \rightarrow P + P(O)Ph_3$). The ketone side-product P' was proposed to be formed through a four-membered endoperoxide intermediate D . Scheme 2 provides a general mechanism for this Cu-catalyzed aerobic vinylogous oxidation reaction, but the details of each elementary step are unknown. Besides, the origin of regioselectivity and the role of copper catalyst remain elusive. Furthermore, the inertness of γ,γ -dialkyl-substituted

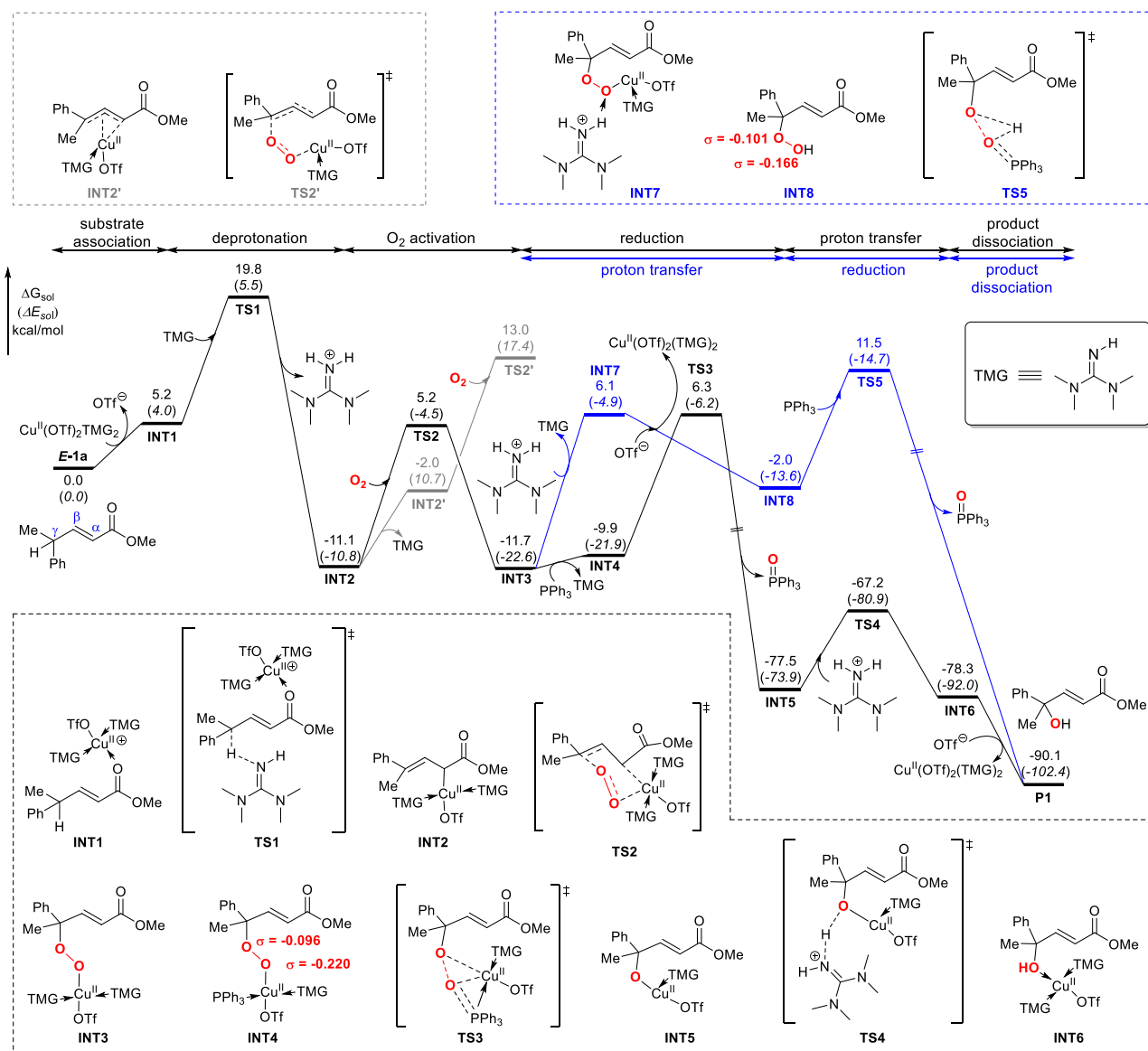


Figure 1. Computed energy profile of copper-catalyzed vinylogous aerobic oxidation of α,β -unsaturated ester. Relative free energies (electronic energies) are in kcal/mol. The Hirshfeld charges of O atoms (highlighted in red) on INT4 and INT8 are listed.

α,β -unsaturated compounds toward the aerobic oxidation reaction and the ineffectiveness of $P(OEt)_3$ as reducing agent have not been fully understood. The understanding of the reaction mechanism is essential for further reaction development. Herein, we perform density functional theory (DFT) calculations¹¹ on this Cu-catalyzed vinylogous aerobic oxidation reaction to elucidate the detailed reaction mechanism, to explore the role of copper catalyst and phosphine, and to understand the observed regioselectivity and side-product formation.

Results and discussion

The resting state of copper catalyst. The $Cu^{II}(OTf)_2$ catalyzed reaction of methyl-(*E*)-4-phenylpent-2-enoate *E-1a* with 1-equivalent TMG and 1-equivalent PPh_3 was selected as a representative case for the DFT calculations (Scheme 3a). We first examined the resting state of the copper catalyst. The $Cu^{II}(OTf)_2$ used in the experiment could be coordinated to the TMG base, the reducing agent PPh_3 or the solvent THF. As shown in Scheme 3b,c, the coordination of one TMG molecule to the $Cu^{II}(OTf)_2$ complex is exergonic by 33.9 kcal/mol. The subsequent coordination of a second TMG molecule to form the $Cu^{II}(OTf)_2(TMG)_2$ complex would release 22.1 kcal/mol of energy. The computational results suggest TMG is a stronger ligand than PPh_3 or THF. The binding with one molecule of PPh_3 or THF is less favorable than that of TMG by 3.1 or 22.4 kcal/mol, respectively. In addition, the generation of cationic copper species from the dissociation of an OTf^- anion of the corresponding neutral copper catalysts are all endergonic (Scheme S1). Thus, the four-coordinated $Cu^{II}(OTf)_2(TMG)_2$ (Scheme 3c) is considered to be the resting state of the copper catalyst in this reaction.

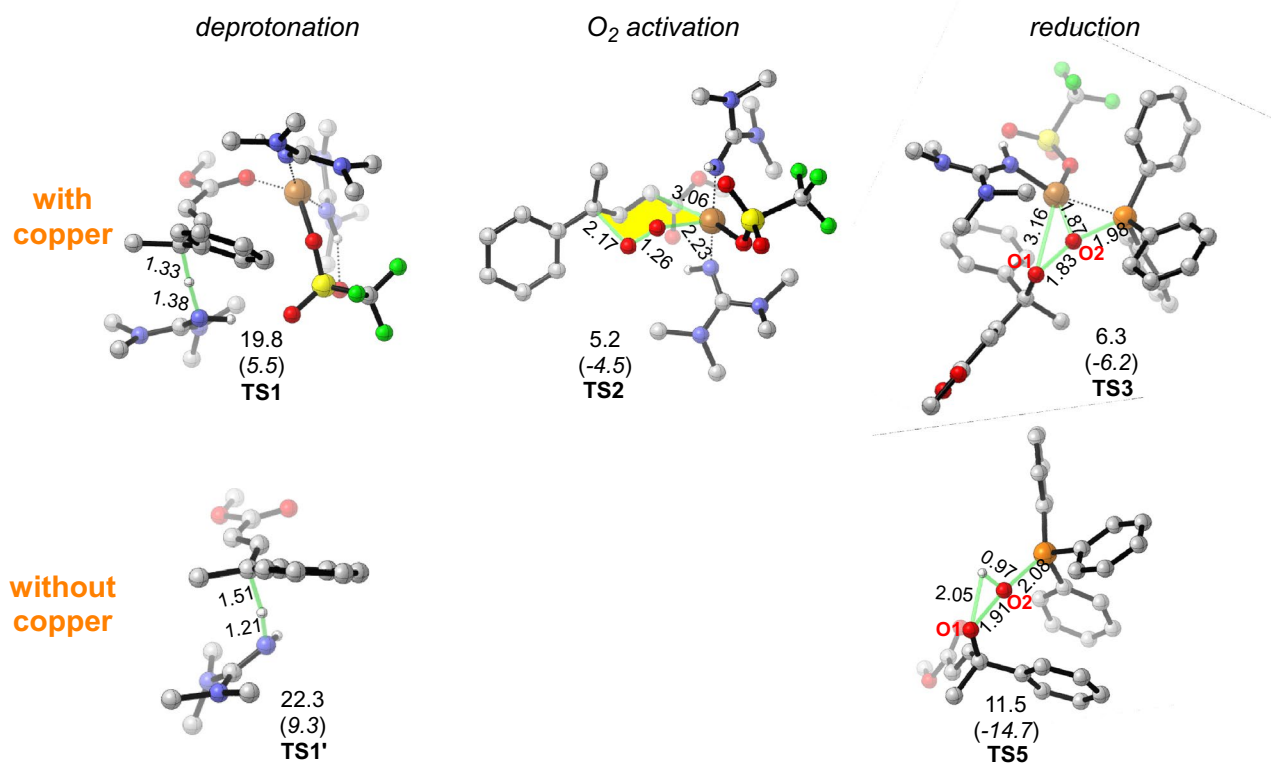


Figure 2. The deprotonation, O₂ activation and reduction transition states. Relative free energies (electronic energies) are in kcal/mol. The bond distances are given in Angstroms (Å). Note CYLview, 1.0b, <https://www.cylview.org/download.html>.

Reaction mechanism of copper-catalyzed γ -hydroxylation. Having determined the resting state of the copper catalyst, we then explored the mechanism of each elementary reaction step (i.e. deprotonation, O₂ activation, and reduction) of the copper-catalyzed γ -hydroxylation of *E-1a*. For each step (except for O₂ activation), both reaction pathways with and without the involvement of copper catalyst were computed to examine the role of copper catalyst.

As of the deprotonation step, the direct deprotonation of substrate *E-1a* by the base (TMG) via TS1' in the absence of copper catalyst requires an energy barrier of 22.3 kcal/mol and this step is energetically uphill by 17.0 kcal/mol, which is thermodynamically unfavorable (Scheme S2). In the copper involved pathway as shown in Fig. 1, the Cu^{II}(OTf)₂(TMG)₂ catalyst first dissociates an OTf⁻ ligand and binds with *E-1a*, generating a cationic copper-substrate species INT1. Subsequently, TMG abstracts a proton from INT1 via transition state TS1 with a free energy barrier of 19.8 kcal/mol and leads to a stable Cu^{II} σ -complex, INT2 (-11.1 kcal/mol). The computational results thus suggest that the coordination of copper with the carbonyl group facilitates the deprotonation of *E-1a* and the formation of stable σ -complex. Further Hirshfeld population analysis demonstrates the C _{γ} hydrogen atoms carries more positive charges when copper catalyst is bound to *E-1a* (Scheme S2). This indicates that the polarity-induced effect by the copper catalyst makes the hydrogen more acidic and thus easier to be activated^{49–51}. Hence, copper acts as an acid Lewis to mediate the first deprotonation step.

Following the deprotonation step, the molecular oxygen approaches the Cu^{II} center and attacks the C _{γ} of *E-1a* substrate in a concerted manner via a six-membered chair-like transition state (TS2, Fig. 2) which leads to a peroxide bridge between Cu and substrate^{52–55}. The distances of O–Cu and O–C _{γ} in TS2 are 2.23 and 2.17 Å, respectively. Moreover, the O–O bond increases from 1.21 Å in O₂ to 1.26 Å in TS2, which indicates that the O₂ has been activated. This oxygen activation step needs to overcome a free energy barrier of 16.3 kcal/mol and results in a γ -peroxy copper intermediate INT3. To understand the regioselectivity, the formation of α -hydroxylated product by the oxygen addition at the α -carbon via transition state α -TS2 was also calculated (Figure S1). The free energy of α -TS2 is 1.3 kcal/mol higher than that of TS2 which leads to the γ -hydroxylated product, in line with the experimental observation that γ -hydroxylated product is more favorable.

To explore the possibility of oxygen activation by binuclear copper species^{52,53,56–58}, we computed the reactions of O₂ with Cu^{II}(OTf)₂(TMG)₂ and Cu^I(OTf)(TMG)₃, respectively, which afford peroxide binuclear copper compounds (Scheme S3). The former reaction is endergonic with 88.5 kcal/mol and thus can be ruled out. Although the latter one has a relatively low reaction free energy (14.9 kcal/mol), the formation of Cu^I(OTf)(TMG)₃ by the disproportionation of Cu^{II}(OTf)₂(TMG)₂ needs 73.5 kcal/mol of energy which excludes the involvement of Cu^I. The computational results thus suggest that the oxygen molecule is unlikely to be activated by binuclear copper complexes.

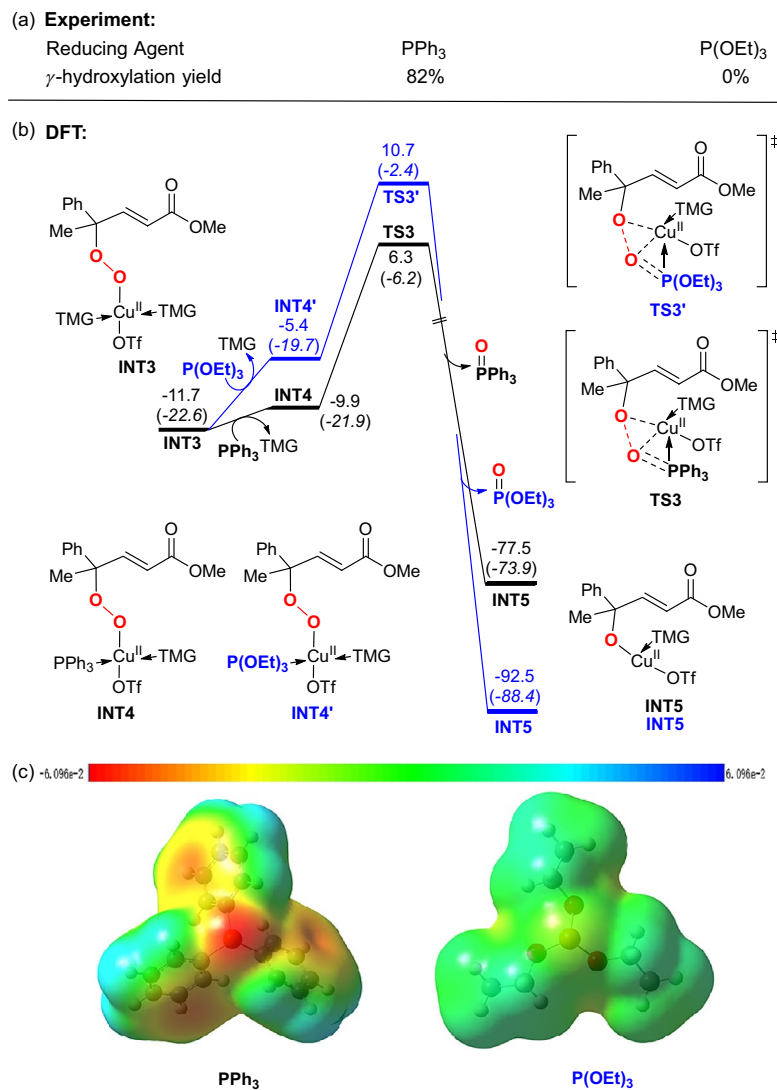


Figure 3. (a) The reaction yields of γ -hydroxylated product using different reducing agents. (b) Theoretically calculated reduction process using different reducing agents. Relative free energies (electronic energies) are in kcal/mol. (c) The electrostatic potential surfaces (ESP) of PPh₃ and P(O)Et₃ mapped between $-6.096e-2$ to $+6.096e-2$. Red as negative extreme and blue as positive extreme. Note GaussView6, <https://gaussian.com/gv6main/>.

After the O₂ activation step, the generated γ -peroxy copper species INT3 is reduced to the γ -hydroxylated product. The reduction process with and without copper (black and blue path in Fig. 1, respectively) was examined. In the black path, INT3 first undergoes rapid ligand exchange with PPh₃ to yield a complex INT4 which is further reduced by PPh₃ through transition state TS3. In this transition state, PPh₃ attacks the distal peroxide oxygen while the copper transfers to the proximal oxygen in a concerted way to yield INT5. The subsequent proton transfer of INT5 via TS4 gives intermediate INT6 which proceeds ligand exchange to release the γ -hydroxylated product and regenerate Cu^{II}(OTf)₂(TMG)₂ catalyst to complete the catalytic cycle. Alternatively, in the reduction process without the participation of copper (blue path), the INT3 first abstracts a proton from the protonated TMG and dissociates from copper to yield the hydroperoxyl compound INT8. Then INT8 undergoes reduction with PPh₃ via a concerted proton shift transition state⁵⁹ (TS5) leading to the γ -hydroxylation product. The calculated activation barriers for the reduction process with and without the involvement of copper (TS3 vs. TS5) are 18.0 and 23.2 kcal/mol, respectively, which indicates that copper facilitates the reduction step. This could be attributed to two main reasons: (1) the incorporation of copper serves to withdraw electron density from the peroxy which helps to polarize the O–O bond as suggested by a larger difference in charges of O atoms on INT4 than that for INT8 (Fig. 1); (2) additional interaction between Cu and the phosphorous atom stabilizes TS3.

Overall, the black path of Fig. 1 that involves substrate association, deprotonation, O₂ activation, reduction, proton transfer and product dissociation was calculated to be the most favorable pathway for the γ -hydroxylation of *E*-1a. The copper-assisted deprotonation step is the rate-determining step, where TMG base plays a pivotal role in hydrogen abstraction. This result coincides with the experimental observation that in the absence of TMG

Entry	Substrates	Products	Time, Yield	Deprotonation TS $\Delta\Delta G^\ddagger$ (kcal/mol)
1	 E-1a		60h, 82%	19.8
2	 E-1b		16h, 90%	17.6
3	 2b		16h, 72%	22.5
4	 E-2a		16h, 0%	24.5

Table 1. The reaction yields and the calculated energy barriers of deprotonation transition states for different substrates.

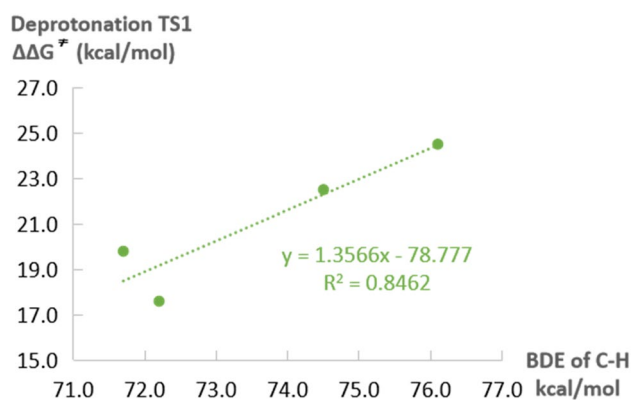


Figure 4. The relationship between deprotonation the energy barriers and the corresponding C–H bond dissociation energy (BDE) for different substrates.

there is no product generated⁴⁵. Furthermore, our computational results suggest the activation of O₂ molecule proceeds via a six-membered chair-like transition state, which is different from the common end-on or side-on O₂ activation model⁷ and accounts for the regioselective γ -carbon activation. In addition, a copper-mediated reduction process in which copper helps to polarize the O–O bond was unveiled by our computation. The reduction of peroxy complexes by phosphine has been reported in many aerobic reactions^{60–65}, while the detailed mechanism is rarely studied. The transition-metal assisted reduction model established in this work provides a possible mechanism for similar reactions. Notably, copper remains as Cu^{II} oxidation state through the whole catalytic cycle and plays vital roles in multiple steps to facilitate the deprotonation, O₂ activation, as well as reduction.

The effect of different reducing agents. The reducing agent plays an important role in this copper-catalyzed vinylogous γ -hydroxylation. A high-yield (82%) of the γ -hydroxylated product was obtained with PPh₃ as a reducing agent, however, the reaction did not occur when PPh₃ was changed to P(OEt)₃ (Fig. 3a). In line with the experiment, our computation in Fig. 3b shows that the reduction with P(OEt)₃ (TS3') is disfavored by 4.4 kcal/mol compared to the corresponding reduction process with PPh₃ (TS3), which supports the PPh₃ is a better reducing agent than P(OEt)₃ for this reaction. The calculated electrostatic potential surfaces (ESPs)^{66–69} in Fig. 3c clearly indicate the P atom of PPh₃ is more electron-rich. Therefore, the PPh₃ could better stabilize the electron-deficient Cu center than P(OEt)₃, accounting for the lower barrier of TS3.

The reactivity of different substrates. The original experimental work reported that γ -aryl- γ -alky-disubstituted α,β -unsaturated compound **E-1a** and γ -aryl- γ -alky-disubstituted β,γ -unsaturated compound **E-1b** are both reactive and generates the same γ -hydroxylated product (Table 1, entry 1 and 2). The γ,γ -dialkyl-

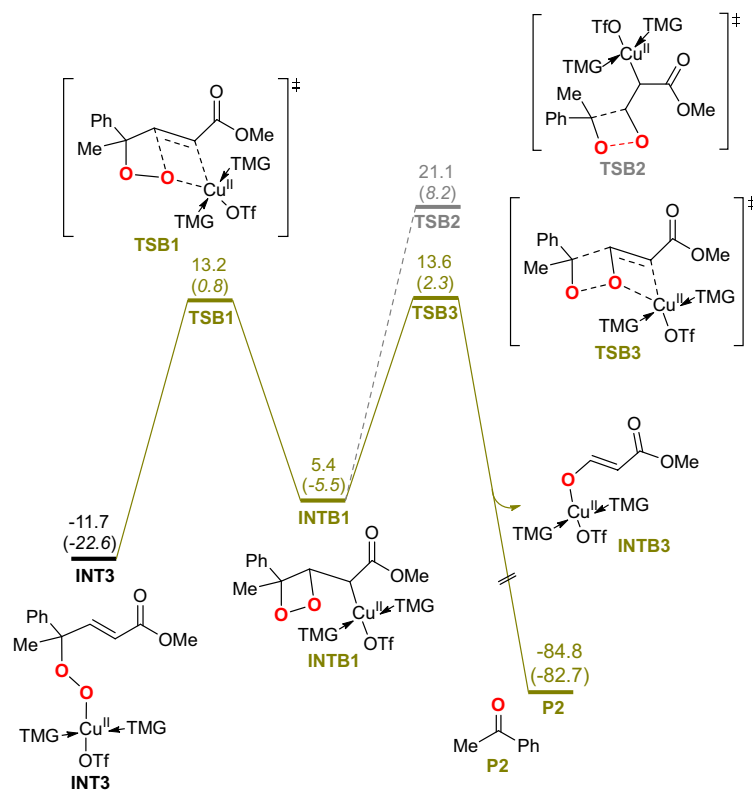


Figure 5. The possible formation routes of acetophenone byproduct. Relative free energies (electronic energies) are in kcal/mol.

substituted β,γ -unsaturated substrate **2b** also exhibits good reactivity (entry 3). However, the γ,γ -dialkyl-substituted α,β -unsaturated compound **E-2a** was completely inert (entry 4). Further computation was performed to understand the observed reactivities of different α,β - or β,γ -unsaturated substrates. As indicated by our DFT studies, the deprotonation process is the rate-determining step. Thus, we examined the deprotonation transition states for different substrates to evaluate their reactivities. The calculated energy barriers of deprotonation follow the order: $\Delta\Delta G^\ddagger(\text{TS1}_{E-1b}) < \Delta\Delta G^\ddagger(\text{TS1}_{E-1a}) < \Delta\Delta G^\ddagger(\text{TS1}_{2b}) < \Delta\Delta G^\ddagger(\text{TS1}_{E-2a})$, which is consistent with the trend of yield (Table 1). To obtain deep insights, the bond dissociation energy (BDE)⁷⁰ of the corresponding C–H bonds (highlighted in red) were calculated to evaluate the intrinsic acidity. As shown in Figs. 4, a good linear association between the deprotonation free energy barriers ($\Delta\Delta G^\ddagger$) and the BDE values were observed. This indicates that the inherent strength of the C–H bond is a key factor affecting the deprotonation process, which is related to the substrate reactivity. In addition, the (*E*)- α,β -unsaturated esters **E-1a** and (*E*)- β,γ -unsaturated esters **E-1b** generated the same γ -hydroxylated product in experiments. Based on the understanding of reaction mechanism and computational results, we concluded that the deprotonation of both (*E*)- α,β -unsaturated ester and (*E*)- β,γ -unsaturated ester would generate the same Cu^{II} σ -complex and thus leads to the same γ -hydroxylated isomer. However, the reactivities of these two substrates (**E-1a** and **E-1b**) are different. **E-1a** has a higher deprotonation energy barrier than **E-1b** by 2.2 kcal/mol corresponding with a lower yield of **E-1a** and further supports the deprotonation is the rate-determining step.

The mechanism of byproduct generation. One of the main problems for the hydroxylation of α,β -unsaturated compounds is the formation of oxidative fragments. In the original experiment, a side product acetophenone was detected and proposed to be generated by oxidative fragmentation of a four-membered endoperoxide intermediate **D** as depicted in Scheme 2. We also explored the formation of acetophenone byproduct. As shown in Scheme 2, the main product path and the byproduct path differentiate from the γ -peroxy copper intermediate.

Starting with this intermediate (**INT3**), three possible pathways leading to the acetophenone byproduct were examined (Scheme S4). A reaction pathway involving a peroxide radical^{71–78} which is formed via the homolysis of Cu–O bond of **INT3** needs to overcome a reaction energy barrier of 29.2 kcal/mol (path I in Scheme S4). Alternatively, **INT3** could undergo an intramolecular alkene insertion into the Cu–O bond via **TSB1** to form four-membered endoperoxide **INTB1** which is similar to the endoperoxide intermediate **D** proposed in the original experimental work (Fig. 5). But the further homolysis of the C–C and O–O bond of **INTB1** via **TSB2** to cleavage the four-membered ring which affords the byproduct is highly unfavorable with an energy barrier of 32.8 kcal/mol. Instead, our computational results demonstrated that copper can facilitate the cycloelimination process by transferring to the β -oxygen atom of endoperoxide (**TSB3**) to maintain the conjugated α,β -unsaturated

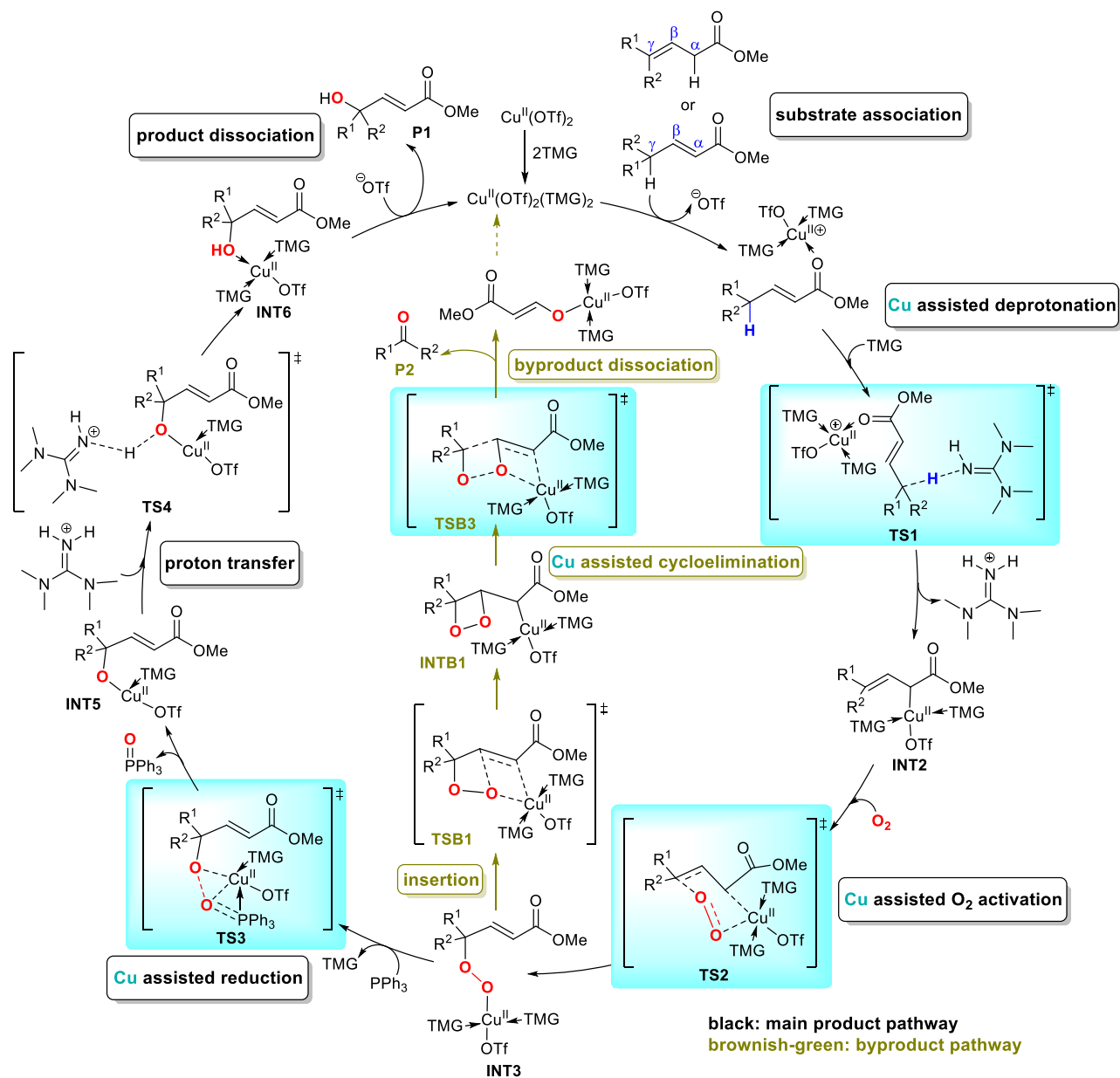


Figure 6. The proposed catalytic cycle for the copper-catalyzed vinylogous aerobic oxidation of α,β - and β,γ -unsaturated compounds.

structure, lowering the activation barrier by 7.5 kcal/mol. The direct cycloelimination of four-membered peroxide complexes was proposed in many works^{79–83} and our results suggested a possible role of transition metal to facilitate the oxidative fragmentation process and to provide the theoretical basis for further reaction improvement.

Conclusion

In summary, we have conducted DFT studies on the Cu-catalyzed vinylogous aerobic oxidation of γ,γ -disubstituted α,β - and β,γ -unsaturated compounds. As summarized in Fig. 6, computational results unveiled a detailed reaction mechanism of γ -hydroxylation reaction that includes six steps: substrate association, deprotonation, O_2 activation, reduction, proton transfer and product dissociation (black path), and the deprotonation is the rate-determining step. The regioselectivity is controlled by the O_2 activation step which prefers to proceed via a six-membered chair-like transition state, leading to a γ -oxidation intermediate. Besides, the inefficiency of $\text{P}(\text{OEt})_3$, and inertness of γ,γ -dialkyl substituted β,γ -unsaturated ester were also understood by computations. A pathway consisting of intramolecular alkene insertion, cycloelimination, and product dissociation (brownish-green path) was revealed to account for the acetophenone byproduct generation. The understanding of the reaction mechanism laid a theoretical foundation for further reaction development.

The copper retains the +2 oxidation state (Cu^{II}) and participates in the whole catalytic cycle of both main product and byproduct formation. Notably, it plays vital roles in multiple steps: (1) facilitates the substrate

deprotonation by increasing the acidity of C–H; (2) activates O₂ via a six-membered chair-like model which is different from the common end-on or side-on O₂ activation model; (3) assists the reduction of peroxy intermediate through a 1,2-migration transition state; and (4) promotes the cycloelimination of endoperoxide by transferring to oxygen to maintain the conjugated α,β -unsaturated structure. The understanding of mechanism for O₂ activation and O–O bond cleavage are essential for the development of transition metal-catalyzed aerobic reactions. The six-membered chair-like transition state for O₂ activation and copper-mediated O–O bond cleavage models (TS3 and TSB3) have not been documented in literature to the best of our knowledge and may provide hints for the mechanistic studies and future development of transition metal-catalyzed aerobic oxidation reactions.

Computational details

All the calculations were performed with Gaussian 09 package⁸⁴. Geometries were optimized in gas phase by using unrestricted B3LYP-D3^{85–88} and a mixed basis set of SDD^{89,90} for Cu and P, and 6-31G(d)^{91,92} basis set for all other atoms. Optimized geometries were verified by frequency computations as minima (zero imaginary frequencies) or transition state (a single imaginary frequency) at the same level of theory. The transition states (TSs) were also confirmed by viewing normal mode vibrational vector. Solvent effect was included by single-point energy calculation using SMD model with tetrahydrofuran (THF) as the solvent and B3LYP-D3 method with def2-TZVP basis set for Cu and P, and 6-311+G(d, p) basis set for other atoms^{93–97}. All relative Gibbs free energies and electronic energies (at 298.15 K and 1 atm) were reported in kcal/mol. The Hirshfeld charges⁹⁸ were obtained from the B3LYP-D3 single-point calculation. The 3D structures were generated by CYLview⁹⁹.

Received: 11 August 2020; Accepted: 9 December 2020

Published online: 14 January 2021

References

- Caron, S., Dugger, R. W., Ruggeri, S. G., Ragan, J. A. & Ripin, D. H. B. Large-scale oxidations in the pharmaceutical industry. *Chem. Rev.* **106**, 2943–2989. <https://doi.org/10.1021/cr040679f> (2006).
- Bäckvall, J.-E. *Modern Oxidation Methods* 2nd edn. (Wiley-VCH, Weinheim, 2011).
- Wang, M. *et al.* Sustainable productions of organic acids and their derivatives from biomass via selective oxidative cleavage of C–C bond. *ACS Catal.* **8**, 2129–2165. <https://doi.org/10.1021/cr040679f> (2018).
- Stahl, S. S. Palladium-catalyzed oxidation of organic chemicals with O₂. *Science* **309**, 1824–1826. <https://doi.org/10.1126/science.1114666> (2005).
- Zweig, J. E., Kim, D. E. & Newhouse, T. R. Methods utilizing first-row transition metals in natural product total synthesis. *Chem. Rev.* **117**, 11680–11752. <https://doi.org/10.1021/acs.chemrev.6b00833> (2017).
- Rappoport, Z. & Marek, I. *The Chemistry of Organocopper Compounds* (Wiley, Chichester, 2009).
- Trammell, R., Rajabimoghadam, K. & Garcia-Bosch, I. Copper-promoted functionalization of organic molecules: from biologically relevant Cu/O₂ model systems to organometallic transformations. *Chem. Rev.* **119**, 2954–3031. <https://doi.org/10.1021/acs.chemrev.8b00368> (2019).
- Shang, M., Sun, S.-Z., Wang, H.-L., Wang, M.-M. & Dai, H.-X. Recent progress on copper-mediated directing-group-assisted C(sp²)–H activation. *Synthesis* **48**, 4381–4399. <https://doi.org/10.1055/s-0035-1562795> (2016).
- McCann, S. D. & Stahl, S. S. Copper-catalyzed aerobic oxidations of organic molecules: pathways for two-electron oxidation with a four-electron oxidant and a one-electron redox-active catalyst. *Acc. Chem. Res.* **48**, 1756–1766. <https://doi.org/10.1021/acs.accounts.5b00060> (2015).
- Ryland, B. L. & Stahl, S. S. Practical aerobic oxidations of alcohols and amines with homogeneous copper/TEMPO and related catalyst systems. *Angew. Chem. Int. Ed.* **53**, 8824–8838. <https://doi.org/10.1002/anie.201403110> (2014).
- Allen, S. E., Walvoord, R. R., Padilla-Salinas, R. & Kozlowski, M. C. Aerobic copper-catalyzed organic reactions. *Chem. Rev.* **113**, 6234–6458. <https://doi.org/10.1021/cr300527g> (2013).
- Wendlandt, A. E., Suess, A. M. & Stahl, S. S. Copper-catalyzed aerobic oxidative C–H functionalizations: trends and mechanistic insights. *Angew. Chem. Int. Ed.* **50**, 11062–11087. <https://doi.org/10.1002/anie.201103945> (2011).
- Ryan, M. C., Martinelli, J. R. & Stahl, S. S. Cu-catalyzed aerobic oxidative N–N coupling of carbazoles and diarylamines including selective cross-coupling. *J. Am. Chem. Soc.* **140**, 9074–9077. <https://doi.org/10.1021/jacs.8b05245> (2018).
- Wu, F., Stewart, S., Ariyaratna, J. P. & Li, W. Aerobic copper-catalyzed alkene oxyamination for amino lactone synthesis. *ACS Catal.* **8**, 1921–1925. <https://doi.org/10.1021/acscatal.7b04060> (2018).
- Iron, M. A. & Szpilmann, A. M. Mechanism of the copper/TEMPO-catalyzed aerobic oxidation of alcohols. *Chem.-Eur. J.* **23**, 1368–1378. <https://doi.org/10.1002/chem.201604402> (2017).
- Xu, B. *et al.* Simple copper catalysts for the aerobic oxidation of amines: selectivity control by the counterion. *Angew. Chem. Int. Ed.* **55**, 15802–15806. <https://doi.org/10.1002/anie.201609255> (2016).
- Liu, M. & Li, C.-J. Catalytic Fehling's reaction: an efficient aerobic oxidation of aldehyde catalyzed by copper in water. *Angew. Chem. Int. Ed.* **55**, 10806–10810. <https://doi.org/10.1002/ange.201604847> (2016).
- McCann, S. D. & Stahl, S. S. Mechanism of copper/azodicarboxylate-catalyzed aerobic alcohol oxidation: evidence for uncooperative catalysis. *J. Am. Chem. Soc.* **138**, 199–206. <https://doi.org/10.1021/jacs.5b09940> (2016).
- Xu, B., Lumb, J.-P. & Arndtsen, B. A. A TEMPO-free copper-catalyzed aerobic oxidation of alcohols. *Angew. Chem. Int. Ed.* **54**, 4208–4211. <https://doi.org/10.1002/anie.201411483> (2015).
- Xu, C., Zhang, L. & Luo, S. Merging aerobic oxidation and enamine catalysis in the asymmetric α -amination of β -ketocarboxylates using N-hydroxycarbamates as nitrogen sources. *Angew. Chem. Int. Ed.* **53**, 4149–4153. <https://doi.org/10.1002/anie.201400776> (2014).
- Sasano, Y. *et al.* Highly chemoselective aerobic oxidation of amino alcohols into amino carbonyl compounds. *Angew. Chem. Int. Ed.* **53**, 3236–3240. <https://doi.org/10.1002/anie.201309634> (2014).
- Esguerra, K. V. N., Fall, Y., Petitjean, L. P. & Lumb, J.-P. Controlling the catalytic aerobic oxidation of phenols. *J. Am. Chem. Soc.* **136**, 7662–7668. <https://doi.org/10.1021/ja501789x> (2014).
- Lee, Y. E., Cao, T., Torruellas, C. & Kozlowski, M. C. Selective oxidative homo- and cross-coupling of phenols with aerobic catalysts. *J. Am. Chem. Soc.* **136**, 6782–6785. <https://doi.org/10.1021/ja500183z> (2014).
- Casiraghi, G., Battistini, L., Curti, C., Rasso, G. & Zanardi, F. The vinylogous aldol and related addition reactions: ten years of progress. *Chem. Rev.* **111**, 3076–3154. <https://doi.org/10.1021/cr100304n> (2011).
- Pansare, S. V. & Paul, E. K. The organocatalytic vinylogous aldol reaction: recent advances. *Chem. Eur. J.* **17**, 8770–8779. <https://doi.org/10.1002/chem.201101269> (2011).

26. Roselló, M. S., Pozo, C. & Fustero, S. A decade of advance in the asymmetric vinylogous Mannich reaction. *Synthesis* **48**, 2553–2571. <https://doi.org/10.1055/s-0035-1561650> (2016).
27. Yin, Y. & Jiang, Z. Organocatalytic asymmetric vinylogous Michael reactions. *ChemCatChem*. **9**, 4306–4318. <https://doi.org/10.1002/cctc.201700941> (2017).
28. Lu, Z. & Ma, S. Metal-catalyzed enantioselective allylation in asymmetric synthesis. *Angew. Chem. Int. Ed.* **47**, 258–297. <https://doi.org/10.1002/anie.200605113> (2008).
29. Hartwig, J. F. & Stanley, L. M. Mechanistically driven development of iridium catalysts for asymmetric allylic substitution. *Acc. Chem. Res.* **43**, 1461–1475. <https://doi.org/10.1021/ar100047x> (2010).
30. Weaver, J. D., Recio, A., Grenning, A. J. & Tunge, J. A. C. Transition metal-catalyzed decarboxylative allylation and benzylation reactions. *Chem. Rev.* **111**, 1846–1913. <https://doi.org/10.1021/cr1002744> (2011).
31. Hethcox, J. C., Shockley, S. E. & Stoltz, B. M. Iridium-catalyzed diastereo-, enantio-, and regioselective allylic alkylation with prochiral enolates. *ACS Catal.* **6**, 6207–6213. <https://doi.org/10.1021/acscatal.6b01886> (2016).
32. Qu, J. & Helmchen, G. Applications of iridium-catalyzed asymmetric allylic substitution reactions in target-oriented synthesis. *Acc. Chem. Res.* **50**, 2539–2555. <https://doi.org/10.1021/acs.accounts.7b00300> (2017).
33. Huang, X., Song, L., Xu, J., Zhu, G. & Liu, B. Asymmetric total synthesis of leucosceptroid B. *Angew. Chem. Int. Ed.* **52**, 952–955. <https://doi.org/10.1002/anie.201208687> (2013).
34. Zhao, X., Li, W., Wang, J. & Ma, D. Convergent route to *ent*-kaurane diterpenoids: total synthesis of lungshengenin D and 1 α ,6 α -diacetoxo-*ent*-kaura-9(11),16-dien-12,15-dione. *J. Am. Chem. Soc.* **139**, 2932–2935. <https://doi.org/10.1021/jacs.7b00140> (2017).
35. Chen, W. *et al.* Total synthesis of (–)-vindorosine. *Angew. Chem. Int. Ed.* **56**, 12327–12331. <https://doi.org/10.1002/anie.201707249> (2017).
36. Xie, C., Luo, J., Zhang, Y., Zhu, L. & Hong, R. A chiral pentenolide-based unified strategy toward dihydrocorynantheol, dihydrocorynantheol, protoemetine, protoemetinol, and yohimbane. *Org. Lett.* **19**, 3592–3595. <https://doi.org/10.1021/acs.orglett.7b01573> (2017).
37. Dubost, C., Markó, I. E. & Ryckmans, T. A concise total synthesis of the lichen macrolide (+)-aspicilin. *Org. Lett.* **8**, 5137–5140. <https://doi.org/10.1021/ol0620287> (2006).
38. Fukui, H. & Shiina, I. Asymmetric total synthesis of botcinins C, D, and F. *Org. Lett.* **10**, 3153–3156. <https://doi.org/10.1021/ol801066y> (2008).
39. Jang, W. J., Song, S. M., Park, Y. & Yun, J. Asymmetric synthesis of γ -hydroxy pinacolboronates through copper-catalyzed enantioselective hydroboration of α , β -unsaturated aldehydes. *J. Org. Chem.* **84**, 4429–4434. <https://doi.org/10.1021/acs.joc.8b03045> (2019).
40. Kumari, A., Gholap, S. P. & Fernandes, R. A. Tandem IBX-promoted primary alcohol oxidation/opening of intermediate β , γ -diolcarbonate aldehydes to (E)- γ -hydroxy- α , β -enals. *Asian J.* **14**, 2278–2290. <https://doi.org/10.1002/asia.201900421> (2019).
41. Son, E. C., Lee, J. & Kim, S.-G. Base-promoted cycloaddition of γ -hydroxy- and δ -hydroxy- α , β -unsaturated carbonyls with azoallyl cations: rapid synthesis of N O-heterocycles. *Eur. J. Org. Chem.* **20**, 3090–3100. <https://doi.org/10.1002/ejoc.20200368> (2020).
42. Schuppe, A. W. & Newhouse, T. R. Assembly of the limonoid architecture by a divergent approach: total synthesis of (\pm)-andirolide N via (\pm)-8 α -hydroxycarapin. *J. Am. Chem. Soc.* **139**, 631–634. <https://doi.org/10.1021/jacs.6b12268> (2017).
43. Masamune, S., Brooks, D. W., Morio, K. & Sobczak, R. L. Construction of the 1,5-methano [10] annulene (bicyclo [5.3.1]-undeca-1,3,5,7,9-pentaene) System. *J. Am. Chem. Soc.* **98**, 8277–8279. <https://doi.org/10.1021/ja00441a074> (1976).
44. Jackson, R. W., Higby, R. G., Gilman, J. W. & Shea, K. J. The chemistry of C-aromatic taxane derivatives atropisomer control of reaction stereochemistry. *Tetrahedron* **48**, 7013–7032. [https://doi.org/10.1016/S0040-4020\(01\)91211-6](https://doi.org/10.1016/S0040-4020(01)91211-6) (1992).
45. Zhang, H.-J. *et al.* Copper-catalyzed vnylogous aerobic oxidation of unsaturated compounds with air. *J. Am. Chem. Soc.* **140**, 5300–5310. <https://doi.org/10.1021/jacs.8b01886> (2018).
46. Jiang, Y.-Y. *et al.* Mechanism of Cu-catalyzed aerobic C(CO)–CH₃ bond cleavage: a combined computational and experimental study. *ACS Catal.* **9**, 1066–1080. <https://doi.org/10.1021/acscatal.8b03993> (2019).
47. Zhang, Q. *et al.* Mechanistic study on Cu(II)-catalyzed oxidative cross-coupling reaction between aenes and boronic acids under aerobic conditions. *J. Am. Chem. Soc.* **140**, 5579–5587. <https://doi.org/10.1021/jacs.8b01896> (2018).
48. Thongkam, P. *et al.* Pyridine–triazole ligands for copper-catalyzed aerobic alcohol oxidation. *RSC Adv.* **5**, 55847–55855. <https://doi.org/10.1039/c5ra06933e> (2015).
49. Sibi, M. P. & Cook, G. R. Copper Lewis acids in organic synthesis, in *Lewis Acids in Organic Synthesis* (Wiley-VCH Verlag GmbH, Weinheim, 2000).
50. Gu, Q.-S., Li, Z.-L. & Liu, X. Y. Copper(I)-catalyzed asymmetric reactions involving radicals. *Acc. Chem. Res.* **53**, 170–181. <https://doi.org/10.1021/acs.accounts.9b00381> (2020).
51. Liang, X.-S., Li, R.-D. & Wang, X.-C. Copper-catalyzed asymmetric annulation reactions of carbenes with 2-iminyl- or 2-acyl-substituted phenols: convenient access to enantioenriched 2,3-dihydrobenzofurans. *Angew. Chem. Int. Ed.* **58**, 13885–13889. <https://doi.org/10.1002/anie.201907943> (2019).
52. Tang, X., Wu, W., Zeng, W. & Jiang, H. Copper-catalyzed oxidative carbon–carbon and/or carbon–heteroatom bond formation with O₂ or internal oxidants. *Acc. Chem. Res.* **51**, 1092–1105. <https://doi.org/10.1021/acs.accounts.7b00611> (2018).
53. Mirica, L. M., Ottenwaelder, X. & Stack, T. D. P. Structure and spectroscopy of copper-dioxygen complexes. *Chem. Rev.* **104**, 1013–1046. <https://doi.org/10.1021/cr020632z> (2004).
54. Liang, Y., Wei, J., Qiu, X. & Jiao, N. Homogeneous oxygenase catalysis. *Chem. Rev.* **118**, 4912–4945. <https://doi.org/10.1021/acs.chemrev.7b00193> (2018).
55. Jin, S.-J., Arora, P. K. & Sayre, L. M. Copper-mediated oxygenation of aldehydes and internal Cannizzaro-like rearrangement of phenylglyoxal. *J. Org. Chem.* **55**, 3011–3018. <https://doi.org/10.1021/jo00297a013> (1990).
56. Suzanne, J. B., Spiccia, L. & Tiekink, E. R. T. Binuclear copper(II) complexes of bis(pentadentate) ligands derived from alkyl-bridged bis(1,4,7-triazacyclonane) macrocycles. *Inorg. Chem.* **35**, 1974–1979. <https://doi.org/10.1021/ic951146f> (1996).
57. Worrell, B. T., Malik, J. A. & Fokin, V. V. Direct evidence of a dinuclear copper intermediate in Cu(I)-catalyzed azide-alkyne cycloadditions. *Science* **340**, 457–460. <https://doi.org/10.1126/science.1229506> (2013).
58. Nierengarten, J.-F. *et al.* Dinuclear copper(I) complexes combining bis(diphenylphosphanyl)acetylene with 1,10-phenanthroline ligands. *Eur. J. Inorg. Chem.* **22**, 2665–2673. <https://doi.org/10.1002/ejic.201900335> (2019).
59. Hiatt, R., Richard, S. & Christine, M. The reaction of hydroperoxides with triphenylphosphine. *Can. J. Chem.* **2011**(49), 1707–1711 (2011).
60. Wiklund, P., Karlsson, C. & Levin, M. Determination of hydroperoxide content in complex hydrocarbon mixtures by gas chromatography/mass spectrometry. *Anal. Sci.* **25**, 431–436. <https://doi.org/10.2116/analsci.25.431> (2009).
61. Rosca, D. A., Wright, J. A., Hughes, D. L. & Bochmann, M. Gold peroxide complexes and the conversion of hydroperoxides into gold hydrides by successive oxygen-transfer reactions. *Nat. Commun.* **4**, 2167. <https://doi.org/10.1038/ncomms3167> (2013).
62. Liang, Y.-F. & Jiao, N. Highly efficient C–H hydroxylation of carbonyl compounds with oxygen under mild conditions. *Angew. Chem. Int. Ed.* **53**, 548–552. <https://doi.org/10.1002/anie.201308698> (2014).
63. Liang, Y. *et al.* CsOH catalyzed aerobic oxidative synthesis of *p*-quinols from multi-alkyl phenols under mild conditions. *Sci. China Chem.* **58**, 1334–1339. <https://doi.org/10.1007/s11426-015-5363-4> (2015).

64. Xiang, S. *et al.* Mn-catalyzed highly efficient aerobic oxidative hydroxyazidation of olefins: a direct approach to B-azido alcohols. *J. Am. Chem. Soc.* **137**, 6059–6066. <https://doi.org/10.1021/jacs.5b02347> (2015).
65. Aegurla, B. *et al.* Triethyl phosphite/benzoyl peroxide mediated reductivealkylation of *O*-benzoylhydroxylamines: a cascade synthesis of secondary amides. *Eur. J. Org. Chem.* **27**, 4235–4238. <https://doi.org/10.1002/ejoc.202000611> (2020).
66. Politzer, P. & Truhlar, D. G. *Chemical Applications of Atomic and Molecular Electrostatic Potentials* (Plenum, New York, 1981).
67. Pingale, S. S. Molecular electrostatic potentials concepts and applications. *Phys. Chem. Chem. Phys.* **13**, 15158–15165. <https://doi.org/10.1039/C1CP20071B> (2011).
68. Politzer, P., Grice, M. E., Murray, J. S. & Seminario, J. M. Anomalous stabilizing and destabilizing effects in some cyclic π -electron systems. *Can. J. Chem.* **71**, 1123–1127. <https://doi.org/10.1139/v93-148> (1993).
69. Suresh, C. H., Alexander, P., Vijayalakshmi, K. P., Sajith, P. K. & Gadre, S. R. Use of molecular electrostatic potential for quantitative assessment of inductive effect. *Phys. Chem. Chem. Phys.* **10**, 6492–6499. <https://doi.org/10.1039/b809561b> (2008).
70. Mills, I., Cvitas, T., Homann, K., Kallay, N. & Kuchitsu, K. *Quantities, Units, and Symbols in Physical Chemistry* (Blackwell Scientific Publications, Oxford, 1988).
71. North, G. R., Pyle, J. & Zhang, F. *Tropospheric Chemistry and Composition* (Academic Press, Oxford, 2015).
72. Ingold, K. U. Peroxy radicals. *Acc. Chem. Res.* **2**, 1–9. <https://doi.org/10.1021/ar50013a001> (1969).
73. Dumont, E. *et al.* Probing the reactivity of singlet oxygen with purines. *Nucleic Acids Res.* **44**, 56–62. <https://doi.org/10.1093/nar/gkv1364> (2016).
74. Boess, E. *et al.* Competitive hydrogen atom transfer to oxyl- and peroxy radicals in the Cu-catalyzed oxidative coupling of *N*-aryl tetrahydroisoquinolines using *tert*-butyl hydroperoxide. *ACS Catal.* **6**, 3253–3261. <https://doi.org/10.1021/acscatal.6b00944> (2016).
75. Liang, Y.-F. & Jiao, N. Oxygenation via C–H/C–C bond activation with molecular oxygen. *Acc. Chem. Res.* **50**, 1640–1653. <https://doi.org/10.1021/acs.accounts.7b00108> (2017).
76. Liu, F., Yang, Z., Yu, Y., Mei, Y. & Houk, K. N. Bimodal Evans–Polanyi relationships in dioxirane oxidations of sp^3 C–H: non-perfect synchronization in generation of delocalized radical intermediates. *J. Am. Chem. Soc.* **139**, 16650–16656. <https://doi.org/10.1021/jacs.7b07988> (2017).
77. Zhang, C. & Jiao, N. Dioxxygen activation under ambient conditions: Cu-catalyzed oxidative amidation–diketonization of terminal alkynes leading to α -ketoamides. *J. Am. Chem. Soc.* **132**, 28–29. <https://doi.org/10.1021/ja908911n> (2010).
78. Zhang, C., Xu, Z., Zhang, L. & Jiao, N. Copper-catalyzed aerobic oxidative coupling of aryl acetaldehydes with anilines leading to α -ketoamides. *Angew. Chem. Int. Ed.* **50**, 11088–11109. <https://doi.org/10.1002/ange.201105285> (2011).
79. Adam, W. & Baader, W. J. Effects of methylation on the thermal stability and chemiluminescence properties of 1,2-dioxetanes. *J. Am. Chem. Soc.* **107**, 410–416. <https://doi.org/10.1021/ja00288a022> (1985).
80. Rodríguez, E. & Reguero, M. The DDCI method applied to reactivity: chemiluminescent decomposition of dioxetane. *J. Phys. Chem. A* **106**, 504–509. <https://doi.org/10.1021/jp0117011> (2002).
81. De Vico, L., Liu, Y.-J., Krogh, J. W. & Lindh, R. Chemiluminescence of 1,2-dioxetane. Reaction mechanism uncovered. *J. Phys. Chem. A* **111**, 8013–8019. <https://doi.org/10.1021/jp074063g> (2007).
82. Farahani, P., Roca-Sanjuán, D., Zapata, F. & Lindh, R. Revisiting the nonadiabatic process in 1,2-dioxetane. *J. Chem. Theory Comput.* **9**, 5404–5411. <https://doi.org/10.1021/ct4007844> (2013).
83. Vacher, M. *et al.* Chemi- and bioluminescence of cyclic peroxides. *Chem. Rev.* **118**, 6927–6974. <https://doi.org/10.1021/acs.chemrev.7b00649> (2018).
84. Frisch, M. J., Trucks, G. W., Schlegel, H. B., Scuseria, G. E., Robb, M. A., Cheeseman, J. R., Scalmani, G., Barone, V., Mennucci, B., Petersson, G. A., Nakatsuji, H., Caricato, M., Li, X., Hratchian, H. P., Izmaylov, A. F., Bloino, J., Zheng, G., Sonnenberg, J. L., Hada, M., Ehara, M., Toyota, K., Fukuda, R., Hasegawa, J., Ishida, M., Nakajima, T., Honda, Y., Kitao, O., Nakai, H., Vreven, T., Montgomery, J. A., Jr., Peralta, J. E., Ogliaro, F., Bearpark, M., Heyd, J. J., Brothers, E., Kudin, K. N., Staroverov, V. N., Keith, T., Kobayashi, R., Normand, J., Raghavachari, K., Rendell, A., Burant, J. C., Iyengar, S. S., Tomasi, J., Cossi, M., Rega, N., Millam, J. M., Klene, M., Knox, J. E., Cross, J. B., Bakken, V., Adamo, C., Jaramillo, J., Gomperts, R., Stratmann, R. E., Yazyev, O., Austin, A. J., Cammi, R., Pomelli, C., Ochterski, J. W., Martin, R. L., Morokuma, K., Zakrzewski, V. G., Voth, G. A., Salvador, P., Dannenberg, J. J., Dapprich, S., Daniels, A. D., Farkas, O., Foresman, J. B., Ortiz, J. V., Cioslowski, J. & Fox, D. J. (Gaussian, Inc., Wallingford, 2009).
85. Becke, A. D. Density-functional exchange-energy approximation with correct asymptotic behavior. *Phys. Rev. A* **38**, 3098–3100. <https://doi.org/10.1103/PhysRevA.38.3098> (1988).
86. Becke, A. D. Density-functional thermochemistry. III. The role of exact exchange. *J. Chem. Phys.* **98**, 5648–5652. <https://doi.org/10.1063/1.464913> (1993).
87. Lee, C., Yang, W. & Parr, R. G. Development of the Colle–Salvetti correlation-energy formula into a functional of the electron density. *Phys. Rev. B* **37**, 785–789. <https://doi.org/10.1103/PhysRevB.37.785> (1988).
88. Grimme, S., Antony, J., Ehrlich, S. & Krieg, H. A consistent and accurate ab initio parametrization of density functional dispersion correction (DFT-D) for the 94 elements H–Pu. *J. Chem. Phys.* **132**, 154104–154119. <https://doi.org/10.1063/1.3382344> (2010).
89. Schaefer, H. F. *Methods of Electronic Structure Theory* (Plenum Press, New York, 1977).
90. Andrae, D., Häußermann, U., Dolg, M., Stoll, H. & Preuß, H. Energy-adjusted ab initio pseudopotentials for the second and third row transition elements. *Theor. Chim. Acta.* **77**, 123–141. <https://doi.org/10.1007/BF01114537> (1990).
91. Ditchfield, R., Hehre, W. J. & Pople, J. A. Self-consistent molecular-orbital methods. IX. An extended Gaussian-type basis for molecular-orbital studies of organic molecules. *J. Chem. Phys.* **54**, 724–728. <https://doi.org/10.1063/1.1677527> (1971).
92. Hariharan, P. C. & Pople, J. A. The influence of polarization functions on molecular orbital hydrogenation energies. *Theor. Chim. Acta.* **28**, 213–222. <https://doi.org/10.1007/BF00533485> (1973).
93. Marenich, A. V., Cramer, C. J. & Truhlar, D. G. Universal solvation model based on solute electron density and on a continuum model of the solvent defined by the bulk dielectric constant and atomic surface tensions. *J. Phys. Chem. B* **113**, 6378–6396. <https://doi.org/10.1021/jp810292n> (2009).
94. Weigend, F. & Ahlrichs, R. Balanced basis sets of split valence, triple zeta valence and quadruple zeta valence quality for H to Rn: design and assessment of accuracy. *Phys. Chem. Chem. Phys.* **7**, 3297–3305. <https://doi.org/10.1039/B508541A> (2005).
95. Krishnan, R., Binkley, J. S., Seeger, R. & Pople, J. A. Self-consistent molecular orbital methods. XX. A basis set for correlated wave functions. *J. Chem. Phys.* **72**, 650–654. <https://doi.org/10.1063/1.438955> (1980).
96. Clark, T., Chandrasekhar, J., Spitznagel, G. W. & Schleyer, P. V. R. Efficient diffuse function-augmented basis sets for anion calculations. III. The 3–21+G basis set for first-row elements, Li–F. *J. Comp. Chem.* **4**, 294–301. <https://doi.org/10.1002/jcc.540040303> (1983).
97. Pritchard, B. P., Altarawy, D., Didier, B., Gibson, T. D., Windus, T. L. A new basis set exchange: An open, up-to-date resource for the molecular sciences community. *J. Chem. Inf. Model.* **59**, 4814–4820. <https://doi.org/10.1021/acs.jcim.9b00725> (2019).
98. Hirshfeld, F. L. Bonded-atom fragments for describing molecular charge densities. *Theor. Chim. Acc.* **44**, 129–138. <https://doi.org/10.1007/BF00549096> (1977).
99. Legault, C. Y. CYLview, 1.0b; Université de Sherbrooke. <http://www.cylview.org> (2009).

Acknowledgements

This work is supported by the National Natural Science Foundation of China (No. 21803047), the China Post-doctoral Science Foundation (No. 2019M650147), the Natural Science Foundation of Guangdong Province (No. 2019A1515011865), Shenzhen Key Laboratory Project (No. ZDSYS20190902093417963) and the Warshel Institute for Computational Biology funding from Shenzhen City and Longgang District.

Author contributions

T.W. performed calculations and data analysis. Y.Z. did the calculation of dimer copper. Y.X. checked for grammatical errors and revised the paper. G.-J.C. proposed this subject and wrote the paper. All authors reviewed the manuscript.

Competing interests

The authors declare no competing interests.

Additional information

Supplementary information is available for this paper at <https://doi.org/10.1038/s41598-020-80188-2>.

Correspondence and requests for materials should be addressed to G.-J.C.

Reprints and permissions information is available at www.nature.com/reprints.

Publisher's note Springer Nature remains neutral with regard to jurisdictional claims in published maps and institutional affiliations.



Open Access This article is licensed under a Creative Commons Attribution 4.0 International License, which permits use, sharing, adaptation, distribution and reproduction in any medium or format, as long as you give appropriate credit to the original author(s) and the source, provide a link to the Creative Commons licence, and indicate if changes were made. The images or other third party material in this article are included in the article's Creative Commons licence, unless indicated otherwise in a credit line to the material. If material is not included in the article's Creative Commons licence and your intended use is not permitted by statutory regulation or exceeds the permitted use, you will need to obtain permission directly from the copyright holder. To view a copy of this licence, visit <http://creativecommons.org/licenses/by/4.0/>.

© The Author(s) 2021